Journal of Magnetism and Magnetic Materials 569 (2023) 170415

Contents lists available at ScienceDirect

Journal of Magnetism and Magnetic Materials

journal homepage: www.elsevier.com/locate/jmmm

Complex interplay between 3d and 4f magnetic systems in multiferroic $DyMnO_3$

A.N. Matveeva [a,*], I.A. Zobkalo [a], M. Meven [b], A.L. Freidman [c,d], S.V. Semenov [c,d], K. Yu. K. Terentjev [c], N.S. Pavlovskiy [c], M.I. Kolkov [c], K.A. Shaykhutdinov [c,d], V. Hutanu [b,1]

[a] Petersburg Nuclear Physics Institute by B.P. Konstantinov of NRC «Kurchatov Institute», 188300 Gatchina, Russia
[b] Institute of Crystallography, RWTH Aachen University and Jülich Centre for Neutron Science at Heinz Maier- Leibnitz Zentrum, Garching, Germany
[c] Kirensky Institute of Physics, Federal Research Center, Krasnoyarsk 660036, Russia
[d] Siberian Federal University, Krasnoyarsk 660041, Russia

ARTICLE INFO

Keywords:
Neutron diffraction
Crystal structure
Multiferroics
Magnetic structure
Manganites

ABSTRACT

Structural and magnetic properties of single crystals of $DyMnO_3$ were investigated by neutron diffraction in order to study the peculiarities of 3d-4f interactions in this compound. Precise magnetic order and its detailed temperature evolution were determined using single crystal neutron diffraction. Elliptical cycloid on manganese subsystem below T_{Ch} = 19 K was confirmed, with temperature decrease the elipticity of the Mn magnetic structure reduces significantly, creating almost circular cycloid. Temperature evolution of the magnetic structure demonstrate specific hysteretic behavior. The results show a complex interplay between transition metal and rare earth magnetic sublattices leading to so-called "Mn- controlled" and "Dy- controlled" magnetic states. The strong and complicate 3d-4f interaction leads to the unusual very slow magnetic structure relaxation.

1. Introduction

Compounds from the orthorhombic manganites family $RMnO_3$ (where R = Tb, Dy, Gd, Ho, Y) are considered to be a typical representatives of multiferroics of type II [1–6]. In these materials ferroelectricity is driven by a particular type of magnetic ordering, which reduces the symmetry of a nonpolar parent phase to a polar magnetic one, and magnetostructural coupling leads to the appearance of an electrically polar state, thus inducing improper ferroelectricity. Close coupling between the magnetic and ferroelectric orders in multiferroics of type II offer the possibility to manipulate one ferroic property by the field of the other one (e.g. electric polarization by magnetic field or magnetic chirality by electric field), thus opening the ways for the development of the new solid state devices. This coupling provides an additional degree of freedom that can be utilized in applications such as magnetoelectric random access memory, in novel magnetic field sensors and other electronic technologies. Most known multiferroics of type II have relatively low values of critical temperatures, below which this coexistence of FE and magnetism is observed. From this point of view, the understanding of microscopic mechanisms of the improper magnetoelectricity in multiferroic materials in general and in $RMnO_3$ series in particular is essential step to the creation of functional materials with the predictable properties.

According to number of theoretical and experimental studies the ferroelectricity in series $RMnO_3$ originates from competing magnetic interactions which produce a long-wavelength AF spin order and lattice modulations with nonzero wave vector [7]. As driving microscopic mechanisms currently considered antisymmetric exchange due to the inverse Dzyaloshinskii-Moriya interaction, symmetric exchange striction, coupling of the magnetic chirality to the crystal as well as a combination of these mechanisms [8–12]. Of great interest is $DyMnO_3$, which develops one of the largest electric polarization among these type of manganites. Long range magnetic order in $DyMnO_3$ is established at T_N = 39 K by the magnetic ordering of Mn^{3+} ions in spin wave structure. An additional transition from non-chiral longitudinal spin density wave modulation to the chiral cycloidal-type structure takes place at T_{Ch} = 19 K [3]. Rare earth (RE) magnetic system becomes polarized at comparatively high temperature by the exchange field of the Mn subsystem and have the same propagation vector, as the Mn one: $\boldsymbol{k}$ = (0 k_y 0). Remarkably the emergence of ferroelectric order coincides with the

* Corresponding author at: Leningradskaya oblast, Gatchina, 1, mkr. Orlova roshcha, PNPI, 188300, Russia.
E-mail address: matveeva_an@pnpi.nrcki.ru (A.N. Matveeva).
[1] Current affiliation: Technical University of Munich, ZWE FRM II, 85748 Garching, Germany.

https://doi.org/10.1016/j.jmmm.2023.170415
Received 19 October 2022; Received in revised form 19 December 2022; Accepted 14 January 2023
Available online 18 January 2023

transition of the Mn magnetic order from the non-chiral type to the chiral one. The relationship between ferroelectric polarization and the cycloidal magnetic structure can be satisfactorily described in the framework of the inverse Dzyaloshinsky-Moria (DMI) model [13,14]. It is worth noting here that Dy^{3+} spontaneous ordering into commensurate antiferromagnetic structure $\boldsymbol{k_{Dy}} = (0\ 1/2\ 0)$, which takes place at ~ 7 K, reduces the ferroelectric polarization significantly [3].

Despite the large number of works on this topic, the precise microscopic mechanism for the occurrence of spontaneous electric polarization in these systems is still under debate. The models of inverse DMI were developed based on the early experimental findings on $TbMnO_3$ [13–15]. In these models, the polarization is proportional to the vector product of the adjacent Mn spins solely $\boldsymbol{P}_e \sim [\boldsymbol{S}_{iMn} \times \boldsymbol{S}_{jMn}]$, and it describes the multiferroic phenomena in $RMnO_3$ rather well. Subsequent studies on the $TbMnO_3$ and especially on $DyMnO_3$ suggest however, that an additional mechanism of polarization emergence may be involved in these compounds [16–19]. Nowadays it is generally assumed, that symmetric exchange-striction between neighboring Dy and Mn ions leads to the enhancement of ferroelectric polarization in $DyMnO_3$: $\boldsymbol{P}_e \sim (\boldsymbol{S}_{Dy} \cdot \boldsymbol{S}_{Mn})$. Thus, the total polarization along the *c*-axis emerges due to two different microscopic mechanisms: from the symmetric exchange-striction between the Dy and Mn sublattices and from the action of inverse DMI within the Mn sublattice. An important issue in this regard is the coherence of the Mn^{3+} and R^{3+} magnetic phases, which plays a crucial role in generating the polarization of the symmetric exchange-striction origin [17–19]. The non-collinear Mn moment alignment results in a ferroelectric state, and then the exchange-striction mechanism enhances the resulting polarization. The chiral incommensurate magnetic ordering of manganese sublattice in $DyMnO_3$ can be regarded as essential prerequisite for the polarization enhancement by the exchange-striction, similar to the situation proposed in the RMn_2O_5 manganites [20]. It is worth mentioning, that after formation of the commensurate magnetic (CM) order of the Dy sublattice below T_N^{Dy} (Dy-Dy interaction becoming dominant), electric polarization is strongly suppressed, emphasizing the importance of the Mn-Dy interactions as the driving mechanism in the polarization enhancement.

It is important to note that $RMnO_3$ compounds, depending on the ionic radius of the RE, have either orthorhombic perovskite structure or hexagonal one under normal growth conditions. $DyMnO_3$ is just located at the boundary of two crystal modifications and, depending on the growth conditions crystalizes in one of these two structures [21–22]. Thus, the RE not only affects the multiferroism of $RMnO_3$, but could also directly influence the crystal symmetry.

Notwithstanding that $DyMnO_3$ could be regarded as a model system for type-II multiferroics [19], the details of magnetic interactions in these systems, which lead to such unusual temperature dependences of magnetic and polarization responses still are not completely known. Our study directed on the elucidation of the features of alignments of two magnetic sub-systems – Mn^{3+} and Dy^{3+} ones, and their mutual influence. As the known crystal symmetry is an important prerequisite for the determining of the magnetic structure, the crystallographic study has been performed by the means of the single crystal neutron diffraction.

2. Experimental

For the measurements we used quality single crystal of $DyMnO_3$. It has the shape of cube with approximate sizes of $3 \times 3 \times 3\ mm^3$.

The neutron diffraction studies were performed at diffractometers HEIDI [23] at the Heinz Maier-Leibnitz Zentrum (MLZ, Garching). This four-circle diffractometer is designed for detailed studies of the structural and magnetic properties of single crystals with hot neutrons.

3. Results and discussions

3.1. Crystal structure of $DyMnO_3$

Generally, in the literature the perovskite orthorhombic space group *Pbnm* is assumed for the crystal structure of $DyMnO_3$ both at room and low temperatures. However, recent detailed study by high resolution neutron and synchrotron powder diffraction at low temperatures, suggested a lowering of the crystal symmetry along with magnetic transitions to the ICM and CM phases to space groups $Pna2_1$ or $P2_1$ [24]. In order to check for these suggested fine atomic displacements, related to the occurrence of the electric polarization in $DyMnO_3$, we performed a number of single crystal neutron diffraction data collects at various low temperatures: 50 K paramagnetic, 25 K Mn-ICM, 8 K – ordering of Dy, and 2.4 K both Dy and Mn ordered and lowest available within used cryostat. The crystal structure of $DyMnO_3$ was explored at the single crystal diffractometer HEIDI with wavelength $\lambda = 0.556$ Å in order to reduce the parasitic effect of absorption on Dy. The crystal structure refinement then was performed using FullProf suite [25]. According to our results, the orthorhombic space group *Pbnm* [Fig. 1] describes well the crystal structure in $DyMnO_3$ at all these temperatures. Neither significant refinement quality or goodness of fit changes in dependence on the temperature, no crystal structure parameters change was observed. Both fractional atomic positions for all atoms and isotropic/anisotropic displacement parameters differ by less than one standard deviation between paramagnetic and highly ordered magnetic temperatures. The obtained atomic positions for 2.4 K are shown (in Table 1). Oxygen content obtained was equal to stoichiometry. Presented here crystal structure parameters obtained by the low-temperature single crystal neutron diffraction are in a good agreement with those reported for $DyMnO_3$ previously by other methods like neutron powder diffraction [24] or single crystal X-ray diffraction [26]. We did not detect neither additional Bragg reflections, forbidden in *Pbnm* group, nor splitting of the measured reflections. We consider that most probably, because of the limitation of the method (lower resolution using hot neutrons), our results could not either confirm, no disaffirm the newly suggested in [24] fine atomic displacement and related symmetry lowering. On the other side, our results clearly show, that traditionally considered space group *Pbnm* still describes well the average symmetry in $DyMnO_3$ at low temperatures in different magnetic states.

3.2. Temperature evolution of the magnetic structure

Investigations of the magnetic structure were carried both in cooling and heating mode. Thermal evolution of the magnetic structure of $DyMnO_3$ can be conveniently traced on the thermal dependence of the satellite $(2\ k_y\ 1)$. The onset of the magnetic ordering was observed at $T_N^{Mn} \approx 38$ K with propagation vector $\boldsymbol{k}^{Mn} = (0\ k_y\ 0)$, $k_y = 0.355(2)$, which is in a good agreement with previous works [3,16]. While cooling below T_N^{Mn}, the intensity of this satellite increases gradually down to ~ 19 K, and then a steep increase of the intensity is observed by further temperature decrease [Fig. 2(a), where this mode labeled as CM42]. This rapid increase is connected to the ordering of the Dy magnetic sublattice induced by Mn ordered sublattice with the same propagation vector $\boldsymbol{k}^{Mn}$ as observed from the resonant X-ray magnetic scattering (XRMS) on the L-edge of Dy [18,16,27]. Our observations from [Fig. 2(a)] are in a good agreement with previously reported synchrotron data, but also neutron scattering results [28]. Remarkably, this temperature (19 K) coincides with the transition from longitudinal spin wave order of Mn to the cycloidal one and also to the temperature T_{CE} where the ferroelectric transition takes places [2,3]. Below $T \sim 6.5$ K the intensity of the ICM satellite drops sharply to the value similar to that observed at temperatures above 27 K characteristic to the ordered Mn lattice only. At this temperature $T_N^{Dy} \sim 6.5$ K the spontaneous ordering of the rare earth magnetic system into an independent CM AFM structure with

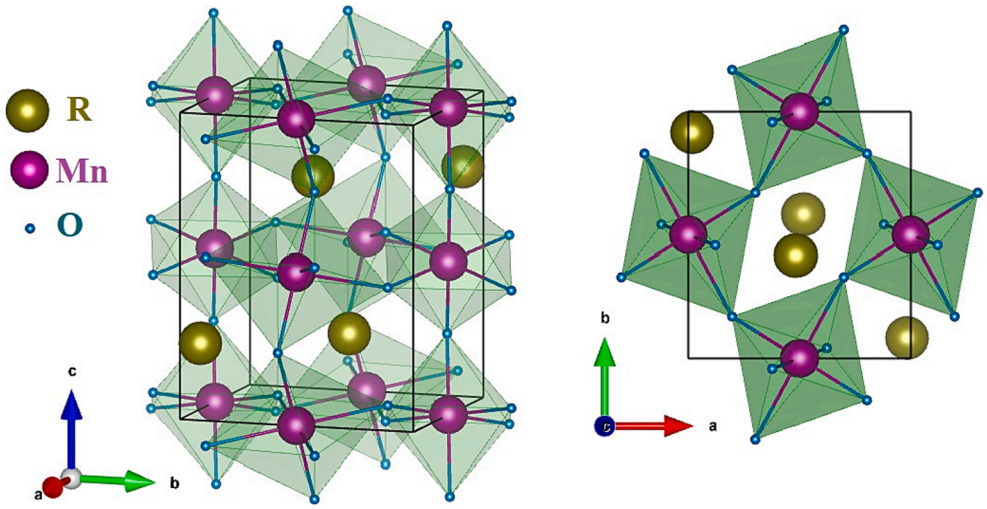

Fig. 1. $RMnO_3$ distorted perovskite crystal structure within space group *Pbnm*.

Table 1
Fractional atomic positions in $DyMnO_3$ temperature 2.4 K resulted from the structural refinement in space group *Pbnm*, determined by single crystal neutron diffraction.

a = 5.269(7), b = 5.845(4), c = 7.331(4) Å			
Atom	x	y	z
Dy, 4c	−0.0180(2)	0.0829(2)	0.25
Mn, 4b	0.5	0	0
O1, 4c	0.1088(9)	0.4622(4)	0.25
O2, 8d	0.7022(5)	0.3276(5)	0.0527(6)
$R_F = 4.49$			

propagation vector $\boldsymbol{k}^{Dy} = (0\ 0.5\ 0)$ takes place. In cooling mode observed in our crystal ICM wave vector component k_y related to the Mn ordering keeps its initial value $k_y = 0.355(2)$ unchanged between 38 and ~ 28 K in good agreement to the previous neutron diffraction study [28]. This behavior is somehow different to that resulting from the observation of the crystal lattice modulation peak with double vector component 2^*k_y by synchrotron scattering [8,16,27]. In the mentioned synchrotron studies a continuous change of k_y between the T_N^{Mn} and T_{Ch} is reported; this difference can be traced to the fact that those measurements were performed in the heating mode, which we will discuss later. Below 28 K k_y starts gradually change from 0.355 to 0.37 at 19 K.

Below this temperature, the wave vector remains constant while cooling down to T_N^{Dy}, where it jumps abruptly to value $k_y = 0.405(2)$ [Fig. 2(b)]. The constant k_y value between $T_{Ch} \approx 19$ K and $T_N^{Dy} \approx 6.5$ K agrees well with previous synchrotron and neutron results. However, to the best of our knowledge, the sudden change of the k_y to the value 0.405 below T_N^{Dy} hasn't been reported previously. In the detailed neutron diffraction study of the Mn sublattice in the $DyMnO_3$ [28] a splitting of the k_y into two peaks with $k_{y1} = 0.363$ and $k_{y2} = 0.39$ was observed. Interestingly, that crystal lattice modulations with ICM wave vector $\boldsymbol{k}_l = \boldsymbol{k}^{Dy} + \boldsymbol{k}^{Mn}$, which is induced by a magnetoelastic coupling between Dy and Mn magnetic moments was found below T_N^{Dy} [8]. Observed on single crystals by synchrotron scattering lattice distortion value $k_l = 0.905$ is in a perfect agreement with reported here magnetic vector components $\boldsymbol{k}^{Mn} = 0.405$ and $\boldsymbol{k}^{Dy} = 0.5$ determined below T_N^{Dy} from the neutron diffraction. The observed (in Ref. 27) deviation from that value was attributed to the use of the large mosaic single crystal sample with 90 % isotopically substituted ^{162}Dy. In such a crystal some parts of the sample may still remain not perfectly ordered down to 4 K.

The thermal dependence of the magnetic satellite width is displayed [in Fig. 3(c)]. While cooling, peaks full width at the half maximum (FWHM) stay constant down to $T_N^{Dy} \sim 6.5$ K, when it sharply increases to almost double resolution-limited value. The broadening of the ICM peaks in $DyMnO_3$ below T_N^{Dy} was observed also by the XRMS experiments and was attributed to presence of the narrow dispersion of the wave vectors in the sample rather than the short range correlations [16]. Taking into account that FWHM does not change by further temperature reduction down to 2.5 K our results obtained by neutron diffraction support this assumption. Worth mentioning is, that our limited resolution by using very short neutron wavelength diffraction could not permit the observation of the ICM peak splitting.

In heating mode the temperature dependence of the integrated intensity demonstrates a noteworthy hysteretic behavior comparing to the cooling case (at Fig. 2 this mode labeled as HM42). Looking at the intensity dependence [Fig. 2(a)], one can see that it increases only very slowly above T_N^{Dy} and returns to its previous "cooling mode" value only above ~ 19 K (remarkably coinciding with T_{Ch}). A qualitatively similar (but quantitatively much less pronounced) hysteretic behavior in the intensity of the magnetic satellite $(0, 1, 2)^+$ around 7 K related to the occurrence of the Dy magnetic ordering was reported also from XRMS measurements [16] in principal agreement with our results. The observed hysteresis resembles well the results presented (in Ref. 28) obtained also by the single crystal neutron diffraction. This hysteretic behavior is an additional manifestation of a strong magnetic coupling between Mn and Dy. In cooling mode the Mn subsystem polarizes the Dy one down to T_N^{Dy}, and polarized Dy subsystem has coherent propagation with Mn one, thus this state we will call the "Mn-controlled" one. Then, below T_N^{Dy}, the RE subsystem already has a significant impact on the Mn magnetic ordering, the so cold "Dy-controlled" state established. In the cooling mode this can be shown by the shift of the incommensurate propagation vector and by the broadening of the incommensurate satellite peaks below T_N^{Dy}. In the heating mode the Dy magnetic subsystem preserves its impact on the Mn even after loosing its own CM long range order. It disturbs the Mn magnetic subsystem up to ~ 19 K, which leads to a broadening of the satellites in this region [Fig. 2(c)]. In addition, the Mn propagation vector component k_y^{Mn} has larger values than that during cooling mode almost up to T_N^{Mn} [Fig. 2(b)]. It seems that the "Dy-controlled" state while heating lasts up to higher temperatures than "Mn-controlled" one while cooling.

At the next step we heated the sample from 2.5 K to 20 K, then it was cooled down to 2.5 K and after that it was heated up to 42 K. The resulting evolution of satellite (2 k_y 1) in this case is presented at Fig. 2 (d) − 2(f) (labeled as CM20, the data shown from 7.5 K down to 2.5 K).

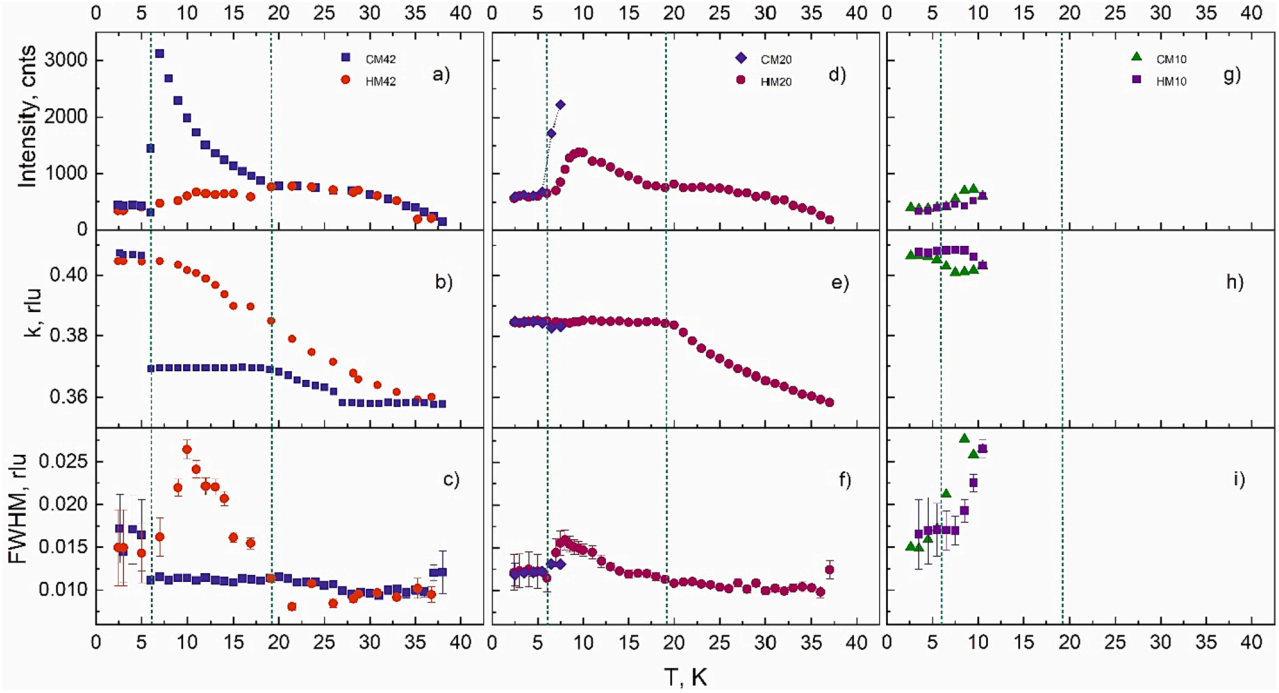

Fig. 2. Temperature evolution of the ICM magnetic Bragg reflection (2 k_y 1) in $DyMnO_3$ by cooling and heating: a), b), c) panels show the evolution of the integrated intensity, wave vector peak full and width at half maximum respectively for the measurement, when the sample was heated from 2.5 K to 42 K (HM42), and then cooled down to 2.5 K (CM42); d), e), f) panels show the evolution of the integrated intensity, wave vector peak full and width at half maximum respectively for the measurement, when the sample was heated from 2.5 K to 20 K, and then cooled down to 2.5 K (CM20) and then heated to 42 K (HM20); g), h), i) panels show the evolution of the integrated intensity, wave vector peak full and width at half maximum respectively for the measurement, when the sample was heated from 2.5 K to 10 K, and then cooled down to 2.5 K(CM10) then heated to 42 K (HM10). The vertical broken lines indicate the observed characteristic magnetic phase transition temperatures.

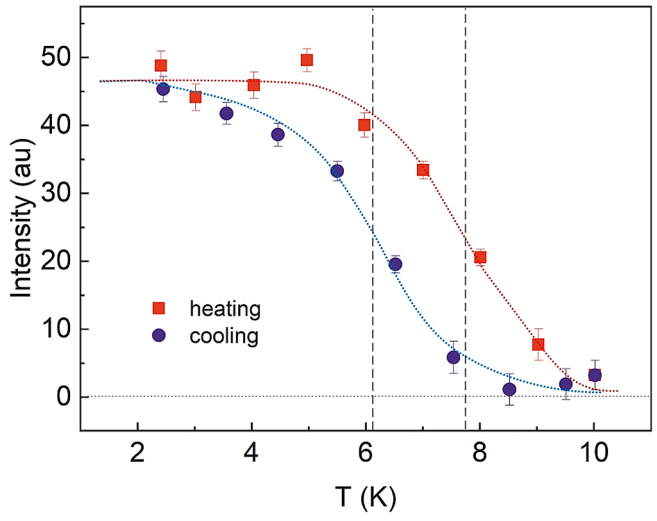

Fig. 3. Temperature dependences of integrated intensity of CM AFM reflection (0 0.5 2) in $DyMnO_3$. Solid lines are guides for the eyes.

Interestingly, the evolution of the intensity of reflection goes almost exactly in the same way as is in case CM42 (Fig. 2(d), while propagation vector component k_y^{Mn} does not change its value of 0.385(2) from 20 K down to 2.5 K (Fig. 2e). The same concerns the width of the satellite (Fig. 2f), which has constant value close to that of CM42. Evolution in the heating mode (labelled HM20) also has interesting features. Intensity dependence of (2 k_y 1) reflection in this measurement mode goes to smooth maximum at ~ 10 K and coincides with HM42 dependence at ~ 19 K. The satellite width also increases noticeably in this region (Fig. 2 (f)). One can suppose, that in this case, by cooling up to 20 K we transformed crystal to "Mn-controlled" almost completely, but there is small admixture of the "Dy-controlled" state. This complex state stabilizes propagation vector $\boldsymbol{k}^{Mn}$ = (0 0.385 0).

For the next measurement we heated the sample to 10 K, then cooled down to 2.5 K (this measurement mode labeled as CM10), and then once more heated up to 42 K (measurement mode HM10). As it can be seen at Fig. 2(g) – 2(f), in this case there is complete coincidence with HM42 for the evolution of all parameters of the magnetic satellite. That is up 10 K the sample stays in "Dy-controlled" state completely.

Fig. 3 shows the temperature dependence of the CM AFM reflections, originating from the Dy^{3+} spontaneous ordering below T_N^{Dy}. The integrated intensity of (0, 0.5, 2) reflection shows a regular hysteretic loop with a width of about 1.8 K between cooling and heating branches in good agreement with previously reported 1.7 K [28]. Taking as transition temperature the inflection point, results in the T_N^{Dy} -cooling ≈ 6.1 K and T_N^{Dy} -heating ≈ 7.9 K. These values are in the good agreement with the most of the previously reported T_N^{Dy} as well. In some published works, an additional critical temperature of about 12 K attributed to polarization flop transition in $DyMnO_3$ is reported. It is worth mentioning, that our single crystal neuron diffraction data on CM and ICM peaks from Mn and Dy magnetic ordering do not show any significant anomalies at that temperature. The only possible trace of such transition in our data may be the broadening of the ICM peak at about 10–12 K while heating [red symbols in the Fig. 2(c)] associated with a small kink in the intensity [red circles in Fig. 2(a)]. No trace of such transition in cooling mode is observable.

3.3. Refinement of magnetic structure from single crystal neutron diffraction data - $DyMnO_3$

In addition to the nuclear peaks, collection of the magnetic Bragg

reflections in $DyMnO_3$ was performed at 2.4 K on diffractometer HEiDi. The data set for the commensurate ordering with wave vector $\boldsymbol{k}_{Dy} = (0\ 0.5\ 0)$ consists of 250 reflections, while for that one for the incommensurate order with $\boldsymbol{k}_{Mn} = (0\ 0.405\ 0)$ only 150 reflections were used for the refinement. Representational analysis shows, that for wave vector $\boldsymbol{k}_{Dy} = (0\ 0.5\ 0)$ the RE site 4c splits into two orbits having the same basis vectors. For Dy^{3+} ions we use the combination of two Γ2 representations with magnetic moments laying in the *ab* plane in the generalized configuration GxAy. It gives satisfactory convergence of the FullProf fit with $\chi^2 = 8.4$ and the resulting moment value $\boldsymbol{M}_{Dy} = (3.51(1), 6.62(6), 0)\ \mu_B$ [see Table III, Fig. 4], which perfectly matches to results (from Refs 16, 25) obtained by the neutron powder diffraction.

As for the incommensurate structure refinement at 2.4 K, for the first attempts we tried to make the refinements with Mn sublattice only, supposing that the Dy subsystem does not give any contribution to the incommensurate order. For the Mn site 4b representation Γ4b decomposes into four irreducible representations Γ1, Γ2, Γ3, Γ4. The ordering of the manganese spins was considered as a combination of two irreducible representations Γ2 and Γ3 with configuration AyAz, as it was proposed previously in Refs. 24, 29. However, this did not lead to a convincing result in terms of fit convergence. In the next step, we included Dy^{3+} sublattice in the fit as well. For $\boldsymbol{k}_{Mn} = (0\ ky\ 0)$, $k_y \neq 0.5$, representational analysis shows that site 4c splits into two orbits, similar to the case of wave vector $\boldsymbol{k}_{Dy} = (0\ 0.5\ 0)$. Thus, Dy^{3+}ordering with configuration GxAy has been added. For elliptical envelope this ensured a good convergence of the fit with $\chi^2 = 2.71$ and the resulting moments values: $\boldsymbol{M}_{Mn} = (0, 2.92(26), 2.77(21))\ \mu_B$, and $\boldsymbol{M}_{Dy} = (2.49(8), 5.57(7), 0)\ \mu_B$ [Table 2, Fig. 5(a)]. We suppose that these two different propagation vectors on Dy3 + subsystem correspond to an incommensurable modulated commensurate magnetic structure. This could be the sequence of situation when incommensurate *k*y component could vary in wide range, up to commensurate value.

For the next step of the investigation of magnetic structure evolution, we made two data collections at $T = 12$ K, approaching to this temperature in cooling and heating mode. As it can be seen in Fig. 3 (a-c), due to a significant difference in the satellite intensity and value of propagation vector, it is natural to anticipate different magnetic structures or, at least different ordered magnetic moments, realized at this temperature in two modes. Judging on the temperature dependences at Fig. 3a-c, it was naturally to suppose that for the structure obtained in heating mode there is only a little (if any) contribution from RE subsystem. For this purpose, about 200 magnetic reflections were collected for both temperature modes. We discuss first the results in cooling mode. Same as in the previous case (2.4 K) we use for refinement configuration AyAz for Mn^{3+} ordering and GxAy for Dy^{3+}. This results in the magnetic moments values: $\boldsymbol{M}_{Mn} = (0, 3.81(14), 1.97(17))\ \mu_B$ and $\boldsymbol{M}_{Dy} = (1.49(6),$ 2.23(7), 0) μ_B (Table III). Note, that obtained overall value of 2.23(7) μ_B for the Dy^{3+} moment at 12 K agrees well with that of 2.5 μ_B obtained in [24]. In the heating mode we began the refinement of the magnetic structure at 12 K considering the Mn moments in AyAz configuration only, without RE contribution. However, this did not lead to a reasonable result. Instead, the inclusion of Dy magnetic system (GxAy) provided good convergence of the fit. Surprisingly, the obtained magnetic moment values in the heating mode almost do not differ (in the frames of experimental accuracy) from those for the cooling mode: $\boldsymbol{M}_{Mn} = (0, 3.74(11), 1.81(16))\ \mu_B$, $\boldsymbol{M}_{Dy} = (1.37(9), 2.18(6), 0)\ \mu_B$. Thus, one received the same magnetic structure for both heating and cooling modes at 12 K [Fig. 7(b)]. At the same time, the temperature hysteresis [Fig. 3 (a-c)] seems to disagree to this result. We believe, that reason for this contradiction is related to the different measurement times used for data collections. In the first case, by the measurement of temperature dependence, the scan of a few satellites at one temperature-point takes just few minutes, including time for the temperature stabilization. Altogether it takes about 2 h to make the full cycle of measurements from 2.4 K to 40 K in heating mode and in particular, about 1 h to make such measurements from 2.4 K to 12 K. Contrarily to that, in the second case, for the measurement of a large number of reflections for magnetic structure refinement, full data set collection takes about 24 hrs. Thus, one can suppose that in our case of $DyMnO_3$ we deal with a very slow magnetic structure relaxation, when the total magnetic structure during some hours transforms from its "Dy controlled" state into the "manganese controlled" one. The contradiction between the obtained value of the incommensurate Dy^{3+} magnetic moment at 2.5 K and significant drop of the intensity of (2 ky 1) reflection, also could be regarded as a sequence of different measurement times for temperature dependence of one reflection and data collection for the magnetic structure refinement. The interesting fact is also, that at $T = 2.4$ K Mn^{3+} refined magnetic moment has a noticeably lower value than at 12 K: 2.92(26) μ_B against 3.81(14) μ_B. At the same time, significant increase of satellite peak width at 2.5 K [Fig. 2(c)] could indicate the correlation length reduction. From another point of view, the broadening of the satellites could be attributed also to the coexistence of few propagation vectors with close ***k***-values. We cannot distinguish between these two possibilities, but both of them surely could be caused by the impact of the RE subsystem on the Mn one. Disturbing influence of the RE probably leads also to the reduction of the effective ordered moment found of the Mn ions at low temperatures.

At the same time, one should paid attention, that the propagation vector of the magnetic structure $\boldsymbol{k}_{Mn}$ remains equal to (0 0.385 0) during the data collection after heating, that is magnetic systems still remains in another local minimum with respect to that one after cooling.

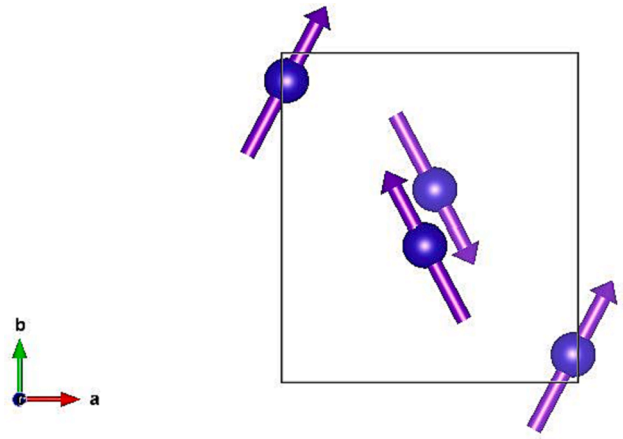

Fig. 4. Magnetic structure model of $DyMnO_3$, only commensurate AFM order on Dy atoms at 2.4 K is shown for sake of clarity.

Table 2
Magnetic structures of $DyMnO_3$ at temperatures 2.5 K and 12 K.

Temperature	Magnetic moment	Wave vector	Mode	M_x, μ_B	M_y, μ_B	M_z, μ_B
2.4 K	Mn	(0 k_y 0)	AyAz	0	2.92 (26)	2.77 (21)
	Dy	(0 k_y 0)	GxAy	2.49 (8)	5.57 (7)	0
	Dy (CM)	(0 0.5 0)	GxAy	3.51 (1)	6.62 (6)	0
12 K (cooling)	Mn	(0 k_y 0)	AyAz	0	3.81 (14)	1.97 (17)
	Dy	(0 k_y 0)	GxAy	1.49 (6)	2.23 (7)	0
12 K (heating)	Mn	(0 k_y 0)	AyAz	0	3.74 (11)	1.81 (16)
	Dy	(0 k_y 0)	GxAy	1.37 (9)	2.18 (6)	0

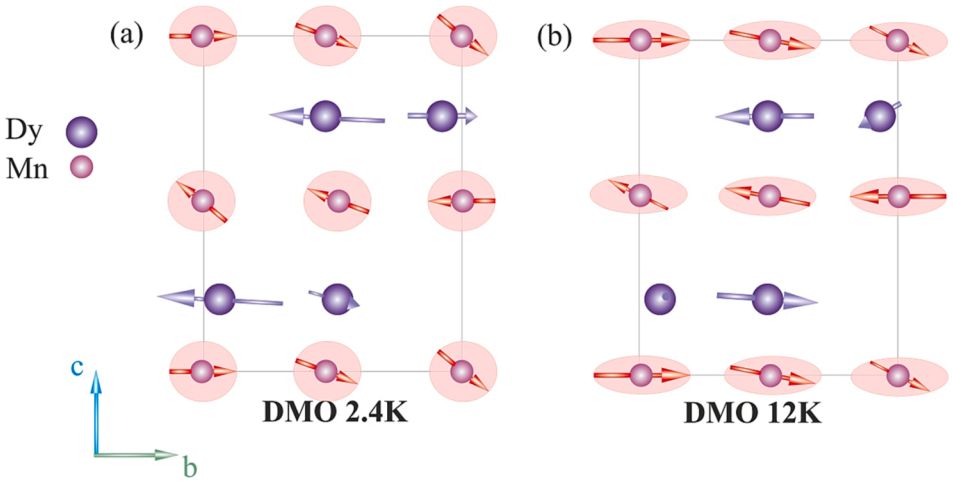

Fig. 5. Incommensurate magnetic structure model (a) $DyMnO_3$ at 2.4 K, (b) $DyMnO_3$ at 12 K.

4. Summary and conclusions

By the single crystal neutron diffraction we performed in-depth studies of the magnetic structure of multiferroic $DyMnO_3$. Our results on the low-temperature crystal structure in $DyMnO_3$ show that reported for the room temperature crystal structure symmetry within orthorhombic space group *Pbnm* describes well the average structure also at very low temperatures in different magnetic phases. No significant magnetic-order-related symmetry change was observed at low temperature within accuracy of the measurements. Measured temperature evolution of the magnetic structure in cooling mode differs significantly from that one measured in heating mode, thus demonstrating specific hysteretic behavior. This kind of evolution confirms the existence of strong RE-Mn coupling, thus leading to the occurrence of two temperature-dependent specific magnetic states: "Mn-controlled" state below $T_N^{Mn} = 38$ K and down to $T_N^{Dy} = 6.5$ K. Then magnetic system of $DyMnO_3$ goes to "Dy-controlled" state. In heating mode magnetic system stays in "Dy-controlled" state up to temperatures much higher than T_N^{Dy} thus demonstrating pronounced temperature hysteresis. This clearly shows that strong RE-Mn coupling persists above as well as below T_N^{Dy}. The precise values of the ordered magnetic moments on Dy and Mn positions respectively were obtained in $DyMnO_3$ from the magnetic structure refinement in both phases: above and below T_N^{Dy}. Interestingly, it was obtained that Dy magnetic subsystem has two propagation vectors simultaneously at low temperature 2.5 K: $\boldsymbol{k}_{Dy1} = (0\ 0.5\ 0)$ and $\boldsymbol{k}_{Dy2} = (0\ k_y\ 0)$.

An attempt to observe a hysteretic dependence of the microscopic magnetic order depending on the heating or cooling prehistory at 12 K showed no difference in the magnetic ordering – the refinement of the magnetic moments gave the same values for both temperature modes. We attribute this to the possible presence of the very slow magnetic relaxation dynamics due to the strong RE-Mn coupling.

It is known from previous investigations [3] that Mn^{3+} ions form chiral elliptical cycloid structure in *bc* plane below 19 K in $DyMnO_3$. Our results reproduce well this physical picture, however we show that with temperature decrease the elipticity of the Mn structure reduces significantly, creating almost circular cycloid.

Our observations provide a direct evidence for the existence of an active interaction between the two magnetic sublattices, which should be considered for the description of the multiferoicity mechanism in $DyMnO_3$.

CRediT authorship contribution statement

A.N. Matveeva: Conceptualization, Methodology, Formal analysis, Data curation, Writing – original draft, Writing – review & editing, Visualization, Investigation. **I.A. Zobkalo:** Conceptualization, Methodology, Validation, Data curation, Writing – review & editing, Supervision, Project administration, Funding acquisition, Investigation. **M. Meven:** Investigation, Formal analysis. **A.L. Freidman:** Resources. **S.V. Semenov:** Resources. **K. Yu. K. Terentjev:** Resources. **N.S. Pavlovskiy:** Resources. **M.I. Kolkov:** Resources. **K.A. Shaykhutdinov:** Resources. **V. Hutanu:** Investigation, Writing – review & editing.

Declaration of Competing Interest

The authors declare that they have no known competing financial interests or personal relationships that could have appeared to influence the work reported in this paper.

Data availability

Data will be made available on request.

Acknowledgments

The authors are grateful to S.V. Gavrilov for the technical assistance. This work was supported by the Russian Foundation for Basic Research grant # 19-52-12047, and DFG grant # SA 3688/1-1, also by Russian Foundation for Basic Research, Government of Krasnoyarsk Territory, Krasnoyarsk Regional Fund of Science to the research projects number 18-42-243024 and 20-42-243008. The neutron data were obtained at the instrument HEiDi operated jointly by RWTH Aachen University and Jülich Centre for Neutron Science within JARA cooperation.

References

[1] T. Kimura, T. Goto, H. Shintani, K. Ishizaka, T. Arima, Y. Tokura, Magnetic control of ferroelectric polarization, Nature 426 (2003) 55, https://doi.org/10.1038/nature02018.
[2] T. Goto, T. Kimura, G. Lawes, A. Ramirez, Y. Tokura, Ferroelectricity and Giant Magnetocapacitance in Perovskite Rare-Earth Manganites Phys, Rev. Lett. 92 (2004), 257201, https://doi.org/10.1103/PhysRevLett.92.257201.
[3] T. Kimura, G. Lawes, T. Goto, Y. Tokura, A.P. Ramirez, Magnetoelectric phase diagrams of orthorhombic $RMnO_3$ (R=Gd, Tb, and Dy), Phys. Rev. B 71 (2005), 224425, https://doi.org/10.1103/PhysRevB.71.224425.
[4] I.A. Sergienko, C. Sen, E. Dagotto, Ferroelectricity in the Magnetic E-Phase of Orthorhombic Perovskites, Phys. Rev. Lett. 97 (2006), 227204, https://doi.org/10.1103/PhysRevLett.97.227204.
[5] S. Picozzi, K. Yamauchi, B. Sanyal, I.A. Sergienko, E. Dagotto, Dual Nature of Improper Ferroelectricity in a Magnetoelectric Multiferroic, Phys. Rev. Lett. 99 (2007), 227201, https://doi.org/10.1103/PhysRevLett.99.227201.
[6] S. Ishiwata, Y. Kaneko, Y. Tokunaga, Y. Taguchi, T.H. Arima, Y. Tokura, Perovskite manganites hosting versatile multiferroic phases with symmetric and

antisymmetric exchange strictions, Phys. Rev. B 81 (2010) 100411(R), https://doi.org/10.1103/PhysRevB.81.100411.
[7] T. Kimura, S. Ishihara, H. Shintani, T. Arima, K.T. Takahashi, K. Ishizaka, Y. Tokura, Distorted perovskite with e_g^1 configuration as a frustrated spin system, Phys. Rev. B 68 (2003) 060403(R), https://doi.org/10.1103/PhysRevB.68.060403.
[8] R. Feyerherm, E. Dudzik, N. Aliouane, D.N. Argyriou, Commensurate Dy magnetic ordering associated with incommensurate lattice distortion in multiferroic $DyMnO_3$, Phys. Rev. B 73 (2006) 180401(R), https://doi.org/10.1103/PhysRevB.73.180401.
[9] M. Kenzelmann, A.B. Harris, S. Jonas, C. Broholm, J. Schefer, S.B. Kim, C.L. Zhang, S.-W. Cheong, O.P. Vajk, J.W. Lynn, Magnetic Inversion Symmetry Breaking and Ferroelectricity in $TbMnO_3$ 087206, Phys. Rev. Lett. 95 (2005), https://doi.org/10.1103/PhysRevLett.95.087206.
[10] G. Lawes, A.B. Harris, T. Kimura, N. Rogado, R.J. Cava, A. Aharony, O. Entin-Wohlman, T. Yildrim, M. Kenzelmann, C. Broholm, A.P. Ramirez, Magnetically Driven Ferroelectric Order in $Ni_3V_2O_8$, Phys. Rev. Lett. 95 (2005), 087205, https://doi.org/10.1103/PhysRevLett.95.087205.
[11] T. Kimura, G. Lawes, A.P. Ramirez, Electric Polarization Rotation in a Hexaferrite with Long-Wavelength Magnetic Structures, Phys. Rev. Lett. 94 (2005), 137201, https://doi.org/10.1103/PhysRevLett.94.137201.
[12] M. Kenzelmann, G. Lawes, A.B. Harris, G. Gasparovic, C. Broholm, A.P. Ramirez, G. A. Jorge, M. Jaime, S. Park, Q. Huang, A.Y. Shapiro, L.A. Demianets, Direct Transition from a Disordered to a Multiferroic Phase on a Triangular Lattice, Phys. Rev. Lett 98 (2007), 267205, https://doi.org/10.1103/PhysRevLett.98.267205.
[13] H. Katsura, N. Nagaosa, A.V. Balatsky, Spin Current and Magnetoelectric Effect in Noncollinear Magnets, Phys. Rev. Lett. 95 (2005), 057205, https://doi.org/10.1103/PhysRevLett.95.057205.
[14] I.A. Sergienko, E. Dagotto, Role of the Dzyaloshinskii-Moriya interaction in multiferroic perovskites, Phys. Rev. B 73 (2006), 094434, https://doi.org/10.1103/PhysRevB.73.094434.
[15] M. Mostovoy, Ferroelectricity in Spiral Magnets, Phys. Rev. Lett. 96 (2006), 067601, https://doi.org/10.1103/PhysRevLett.96.067601.
[16] O. Prokhnenko, R. Feyerherm, E. Dudzik, S. Landsgesell, N. Aliouane, L.C. Chapon, D.N. Argyriou, Enhanced Ferroelectric Polarization by Induced Dy Spin Order in Multiferroic $DyMnO_3$, Phys. Rev. Lett. 98 (2007), 057206, https://doi.org/10.1103/PhysRevLett.98.057206.
[17] R. Feyerherm, E. Dudzik, O. Prokhnenko, D.N. Argyriou, Rare earth magnetism and ferroelectricity in $RMnO_3$, J. Phys.: Conf. Series 200 (2010), 012032, https://doi.org/10.1088/1742-6596/200/1/012032.
[18] H.W. Wang, C.L. Li, S.L. Yuan, J.F. Wang, C.L. Lu, J.-M. Liu, The crucial role of Mn spiral spin order in stabilizing the Dy–Mn exchange striction in multiferroic $DyMnO_3$, Phys. Chem. Chem. Phys. 19 (2017) 3706.
[19] C. Lu, J.-M. Liu, DyMnO3: A model system of type-II multiferroics, Materiomics 2 (2016) 213, https://doi.org/10.1016/j.jmat.2016.04.004.
[20] I.A. Zobkalo, A.N. Matveeva, A. Sazonov, S.N. Barilo, S.V. Shiryaev, B. Pedersen, V. Hutanu, Direct control of magnetic chirality in $NdMn_2O_5$ by external electric field, Phys. Rev. B 101 (2020), 064425, https://doi.org/10.1103/PhysRevB.101.064425.
[21] H.L. Yakel, W.C. Koehler, E.F. Bertaut, E.F. Forrat, On the crystal structure of the manganese(III) trioxides of the heavy lanthanides and yttrium, Acta Crystallogr. 16 (1963) 957, https://doi.org/10.1107/S0365110X63002589.
[22] V.Y. Ivanov, A.A. Mukhin, A.S. Prokhorov, A.M. Balbashov, L.D. Iskhakova, Magnetic Properties and Phase Transitions in Hexagonal $DyMnO_3$ Single Crystals, Phys. Solid State 48 (2006) 1726, https://doi.org/10.1134/S1063783406090186.
[23] M. Meven, A. Sazonov, HEiDi: Single crystal diffractometer at hot source, J. Large-scale Res. Facilities 1 A7 (2015). DOI: 10.17815/jlsrf-1-20.
[24] N. Narayanan, P.J. Graham, N. Reynolds, F. Li, P. Rovillain, J. Hester, J. Kimpton, M. Yethiraj, G.J. McIntyre, W.D. Hutchison, C. Ulrich, Subpicometer-scale atomic displacements and magnetic properties in the oxygen-isotope substituted multiferroic $DyMnO_3$, Phys. Rev. B 95 (2017), 075154, https://doi.org/10.1103/PhysRevB.95.075154.
[25] J. Rodriguez-Carvajal, Recent advances in magnetic structure determination by neutron powder diffraction, Physica B 192 (1993) 55, https://doi.org/10.1016/0921-4526(93)90108-I.
[26] T. Mori, K. Aoki, N. Kamegashira, T. Shishido, T. Fukuda. Mater. Size-dependent structure and magnetic properties of $DyMnO_3$ nanoparticles Lett. 42, 387 (2000). https://doi.org/10.1063/1.4895128.
[27] J. Strempfer, B. Bohnenbuck, M. Mostovoy, N. Aliouane, D. N. Argyriou, F. Schrettle, J. Hemberger, A. Krimmel, M. V. Zimmermann, Absence of commensurate ordering at the polarization flop transition in multiferroic $DyMnO_3$, Phys. Rev. B 75, 212402 (2007). DOI:https://doi.org/10.1103/PhysRevB.75.212402.
[28] T. Finger, K. Binder, Y. Sidis, A. Maljuk, D.N. Argyriou, M. Braden, Magnetic order and electromagnon excitations in $DyMnO_3$ studied by neutron scattering experiments, Phys. Rev. B 90 (2014), 224418, https://doi.org/10.1103/PhysRevB.90.224418.